Energies **2012**, *5*, 2331-2350; doi:10.3390/en5072331

OPEN ACCESS

energies

ISSN 1996-1073

www.mdpi.com/journal/energies

Article

Energy Storage System with Voltage Equalization Strategy for Wind Energy Conversion

Cheng-Tao Tsai

Department of Electrical Engineering, National Chin-Yi University of Technology, Taichung 41170, Taiwan; E-Mail: cttsai@ncut.edu.tw; Tel.: +886-4-23924505 (ext. 7240); Fax: +886-4-23924419

Received: 21 March 2012; in revised form: 29 May 2012 / Accepted: 26 June 2012 / Published: 9 July 2012

Abstract: In this paper, an energy storage system with voltage equalization strategy for wind energy conversion is presented. The proposed energy storage system provides a voltage equalization strategy for series-connected lead-acid batteries to increase their total storage capacity and lifecycle. In order to draw the maximum power from the wind energy, a perturbation-and-observation method and digital signal processor (DSP) are incorporated to implement maximum power point tracking (MPPT) algorithm and power regulating scheme. In the proposed energy storage system, all power switches have zero-voltage-switching (ZVS) feature at turn-on transition. Therefore, the conversion efficiency can be increased. Finally, a prototype energy storage system for wind energy conversion is built and implemented. Experimental results have verified the performance and feasibility of the proposed energy storage system for wind energy conversion.

Keywords: series-connected; perturbation-and-observation; zero-voltage-switching (ZVS)

1. Introduction

A large amount of carbon dioxide produced by combustion of fossil fuels are believed to be responsible for trapping heat in the Earth's atmosphere, resulting in serious greenhouse effects and environmental pollution. This effect is being linked to changes in the Earth's climate. To reduce emissions of carbon dioxide, the demand for renewable energy sources has increased significantly. The typical renewable energy sources include solar, wind and geothermal energies, which have the features of cleanliness and freedom [1], therefore developing renewable and clean energy sources to substitute for fossil fuels has been an important topic. Currently, wind is one of most widely utilized renewable

energies. Wind turbine technology has been undergoing a dramatic development and now is the world's fastest growing energy source [2–6]. However, due to the instability and intermittent characteristics of wind energy, it cannot provide a constant or stable power output. Thus, maximum power point tracking (MPPT) and energy storage are very important technologies. Many MPPT methods have been developed, mostly dominated by a simple perturbation and observation method [7–10]. The method requires the measurement of only a few parameters thus facilitating an MPPT control. As a result, it is often applied to the wind turbine energy for enhancing power capacity.

Batteries are essential elements for wind energy storage applications. Lead-acid batteries connected in series and parallel to supply higher voltage and capacity are utilized in many practical applications, because large amounts of energy can be stored at low cost. However, the differences between battery charge and discharge rates, residual capacities and internal resistance voltage usually cause imbalances in series-connected lead-acid batteries, resulting in a decrease of the total storage capacity and battery lifecycle. Thus, voltage equalization charging techniques for series-connected batteries are becoming important. In general, there are several charging techniques to overcome the voltage imbalances in series-connected batteries. The evolution of charging strategies is as follows:

(1) Dissipative shunting resistor,
(2) Multi-winding transformer, and
(3) Multiple transformers.

The dissipative shunting resistor is an effective voltage equalization method because of its reliability and simplicity [11]. Figure 1 shows a voltage equalization circuit with dissipative resistor.

Figure 1. Equalization circuit of dissipative resistor.

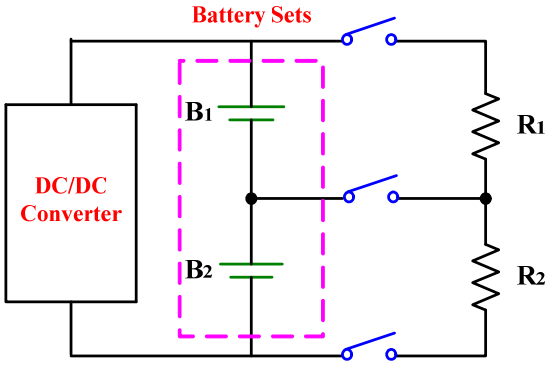

However, the circuit has disadvantages that the dissipative resistor method has poor efficiency and needs many MOSFETs, resulting in complex control. In the multi-winding transformer equalization circuit, a shared transformer has a single magnetic core with secondary taps for each battery, as shown in Figure 2. The multi-winding transformer must be customized according to the number of batteries, which results in this circuit complex and high cost [12]. Figure 3 shows the multiple transformers equalization circuit. In this circuit, several transformers can be used with the same result by coupling the primary windings instead of coupling via a single magnetic core. Compared to the multi-winding transformer scheme, this method is better for modular design, but it is still expensive.

Figure 2. Equalization circuit of multi-winding transformer.

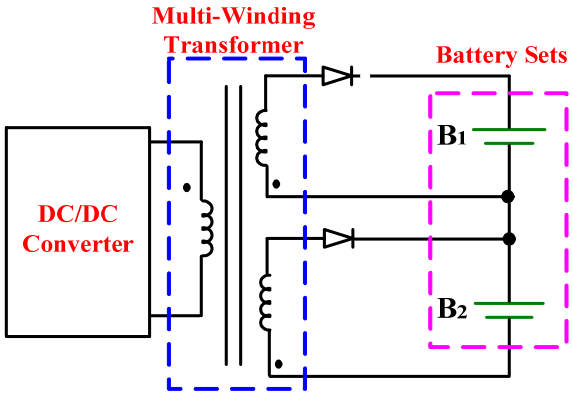

Figure 3. Equalization circuit of multiple transformers.

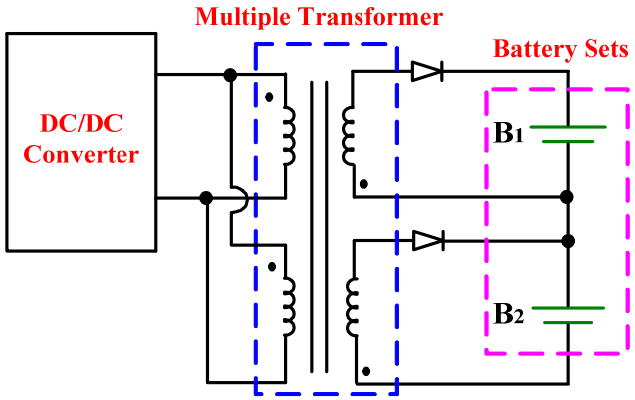

In this paper, an energy storage system with voltage equalization strategy for wind energy conversion is presented, as shown in Figure 4.

Figure 4. Circuit structure of the proposed energy storage system for wind energy conversion.

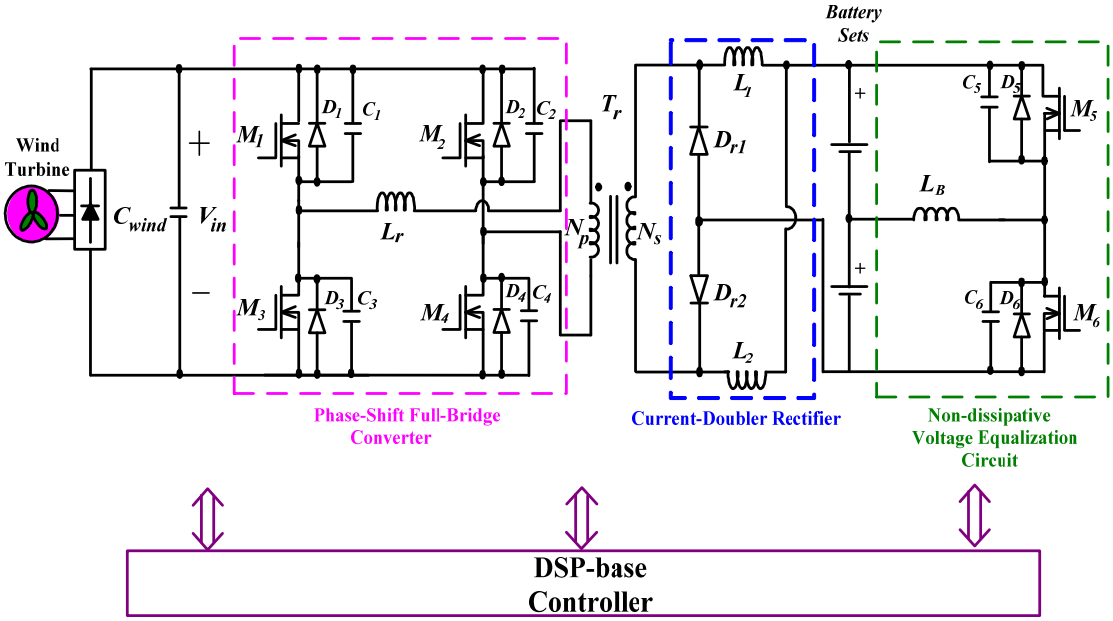

It is composed of a phase-shift full-bridge converter, a current-doubler rectifier and a non-dissipative voltage equalization circuit. The phase-shift full-bridge converter is incorporated with perturbation and observation method to draw the maximum power from the wind turbine energy. In addition, by phase-shift PWM approach, all power switches of full-bridge converter can be operated with a ZVS feature at turn-on transition [13]. In order to reduce charging current ripples of series-connected batteries, the current-doubler rectifier with an interleaved method is implemented. Finally, the non-dissipative voltage equalization circuit is in cascade connection to achieve voltage equalization of series-connected batteries [14,15].

The operational principles of the proposed energy storage system are described in Section 2. The MPPT wind energy and control scheme algorithm is decribed in Section 3. Experimental results obtained from a 600 W prototype with the proposed energy storage system for wind energy conversion are presented in Section 4. Finally, a conclusion is given in Section 5.

2. Operational Principles

For convenience of illustration and analysis, the proposed energy storage system shown in Figure 4 is divided into two operational modes. One is charging mode, the other is voltage equalization mode, as shown in Figure 5.

Figure 5. Two equivalent circuits of the proposed energy storage system: (**a**) charging mode; (**b**) voltage equalization mode.

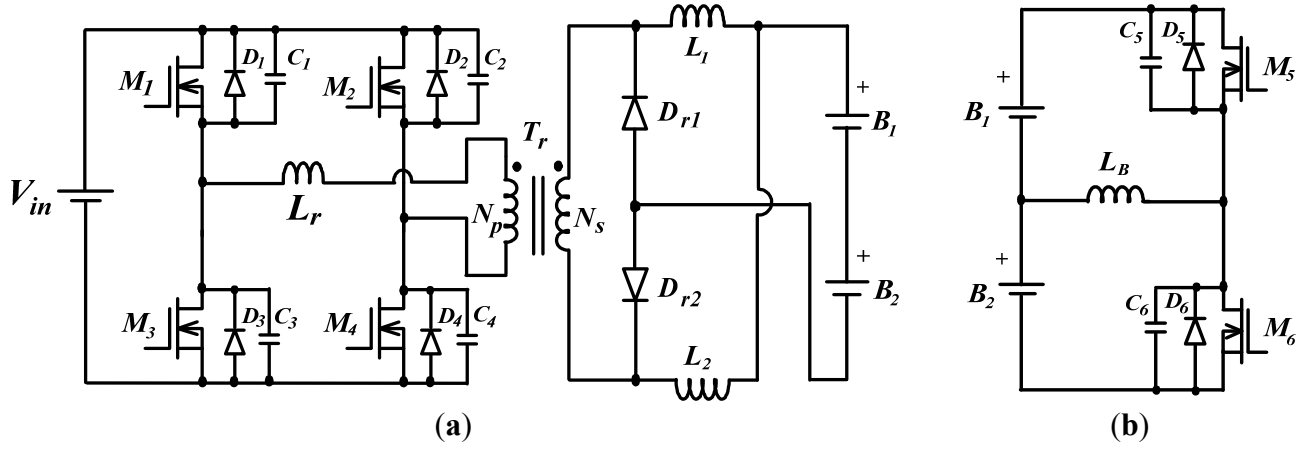

To simplify the description of the operational stages, the following assumptions are made:

(1) To achieve ZVS feature for all power switches of full-bridge converter, the extra resonant inductor (L_r) is usually required.

(2) To analyze the ZVS feature of all power switches (M_1, M_2, M_3, M_4, M_5 and M_6), their body diodes (D_1, D_2, D_3, D_4, D_5 and D_6) and parasitic capacitors (C_1, C_2, C_3, C_4, C_5 and C_6) will be considered at the steady-state operation of the circuit.

Based on the above assumptions, the operational principle of the proposed energy storage system for charging mode and voltage equalization mode can be explained stage by stage as follows:

2.1. Operational Principles of Charging Mode

In the proposed energy storage system, the operation principles of the charging mode over one switching period can be divided into eight stages. Figure 6 shows conceptual voltage and current waveforms relative to key components of the proposed energy storage system at charging mode.

Figure 6. Driving signals of switches (M_1~M_4) and conceptual current and voltage waveforms of key components for charging mode.

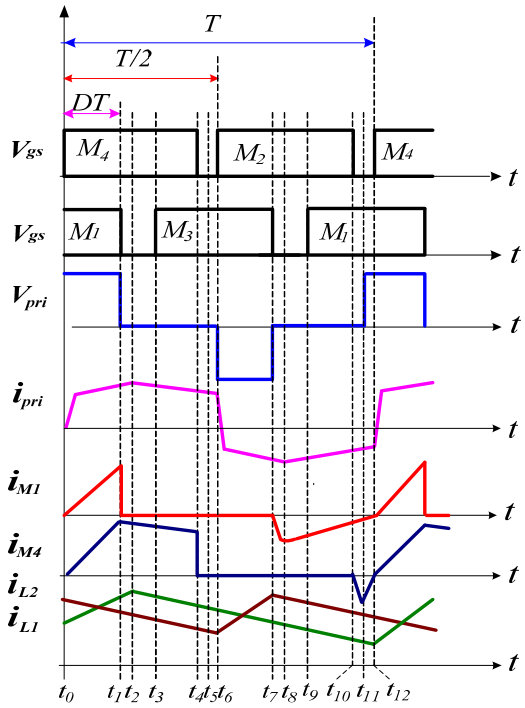

Figure 7 shows its equivalent circuits.

Stage 1 [Figure 7(a), $t_0 \le t < t_1$]:

At time t_0, active switches M_1 and M_4 are conducted, the primary current i_{pri} flows through the path M_1-L_r-T_r-M_4. At secondary side of transformer, a positive voltage V_{sec} crosses the secondary winding of transformer T_r. The rectifier diode D_{r1} is reversely biased and D_{r2} is conducting. During this interval, inductor current i_{L1} flowing through the path B_1-B_2-D_{r2}-Ns-L_1 is linearly increased, and inductor current i_{L2} flowing through the path B_1-B_2-D_{r2}-L_2 is linearly decreased.

Stage 2 [Figure 7(b), $t_1 \le t < t_2$]:

At time t_1, the active switch M_1 is turned off and M_4 is maintained conducting. The parasitic capacitor C_1 of the M_1 is charged to V_{in}, while parasitic capacitor C_3 of the M_3 is discharged down to zero.

Stage 3 [Figure 7(c), $t_2 \le t < t_3$]:

At time t_2, the current i_{pri} forces the body diode D_3 of M_3 conducting and creating a ZVS feature for M_3. At secondary side of transformer, the rectifier diodes D_{r1} and D_{r2} are forward biased. Inductor currents i_{L1} and i_{L2} flow through the rectifier diodes D_{r1} and D_{r2}, respectively.

Stage 4 [Figure 7(d), $t_3 \le t < t_4$]:

At time t_3, the active switch M_3 is turned on under ZVS transition. While the active switch M_4, rectifier diodes D_{r1} and D_{r2} are maintained conducting. During this interval, the inductor current i_{L1} and i_{L2} continue decreasing linearly.

Stage 5 [Figure 7(e), $t_4 \le t < t_5$]:

At time t_4, the active switch M_4 is turned off and M_3 is maintained conducting. The parasitic capacitor C_4 of the M_4 is charged to V_{in}, while parasitic capacitor C_2 of the M_2 is discharged down to zero.

Stage 6 [Figure 7(f), $t_5 \le t < t_6$]:

At time t_5, the current i_{pri} forces the body diode D_2 of M_2 conducting and creating a ZVS feature for M_2. During this interval, the inductor currents i_{L1} and i_{L2} continue decreasing linearly.

Stage 7 [Figure 7(g), $t_6 \le t < t_7$]:

At time t_6, the active switch M_2 is turned on under ZVS transition and the active switch M_3 is maintained conducting. When the energy of resonant inductor L_r is released to zero, the primary current i_{pri} begins reversely flowing through the path M_2-T_r-L_r-M_3. At secondary side of transformer, a negative voltage V_{sec} crosses the secondary winding of transformer T_r. The rectifier diode D_{r2} is reversely biased and D_{r1} is conducting. During this interval, inductor current i_{L2} flowing through the path B_1-B_2-D_{r1}-N_s-L_2 is linearly increased, and inductor current i_{L1} flowing through the path B_1-B_2-D_{r1}-L_1 is linearly decreased.

Stage 8 [Figure 7(h), $t_7 \le t < t_8$]:

At time t_7, the active switch M_3 is turned off and M_2 is maintained conducting. The parasitic capacitor C_3 of the M_3 is charged to V_{in}, while parasitic capacitor C_1 of the M_1 is discharged down to zero.

Stage 9 [Figure 7(i), $t_8 \le t < t_9$]:

At time t_8, the current i_{pri} forces the body diode D_1 of M_1 conducting and creating a ZVS feature for M_1. At secondary side of transformer, the rectifier diodes D_{r1} and D_{r2} are forward biased. Inductor currents i_{L1} and i_{L2} flow through the rectifier diodes D_{r1} and D_{r2}, respectively.

Stage 10 [Figure 7(j), $t_9 \le t < t_{10}$]:

At time t_9, the active switch M_1 is turned on under ZVS transition. While the active switch M_2, rectifier diodes D_{r1} and D_{r2} are maintained conducting. During this interval, the inductor currents i_{L1} and i_{L2} continue decreasing linearly.

Stage 11 [Figure 7(k), $t_{10} \le t < t_{11}$]:

At time t_{10}, the active switch M_2 is turned off and M_1 is maintained conducting. The parasitic capacitor C_2 of the M_2 is charged to V_{in}, while parasitic capacitor C_4 of the M_4 is discharged down to zero.

Stage 12 [Figure 7(l), $t_{11} \le t < t_{12}$]:

At time t_{11}, the current i_{pri} forces the body diode D_4 of M_4 conducting and creating a ZVS feature for M_4. During this interval, the inductor currents i_{L1} and i_{L2} continue decreasing linearly. When active switch M_4 starts conducting again at the end of *Stage 12*, the charging operation of energy storage system over one switching cycle is completed.

Figure 7. Equivalent circuits of operating stages for charging mode.

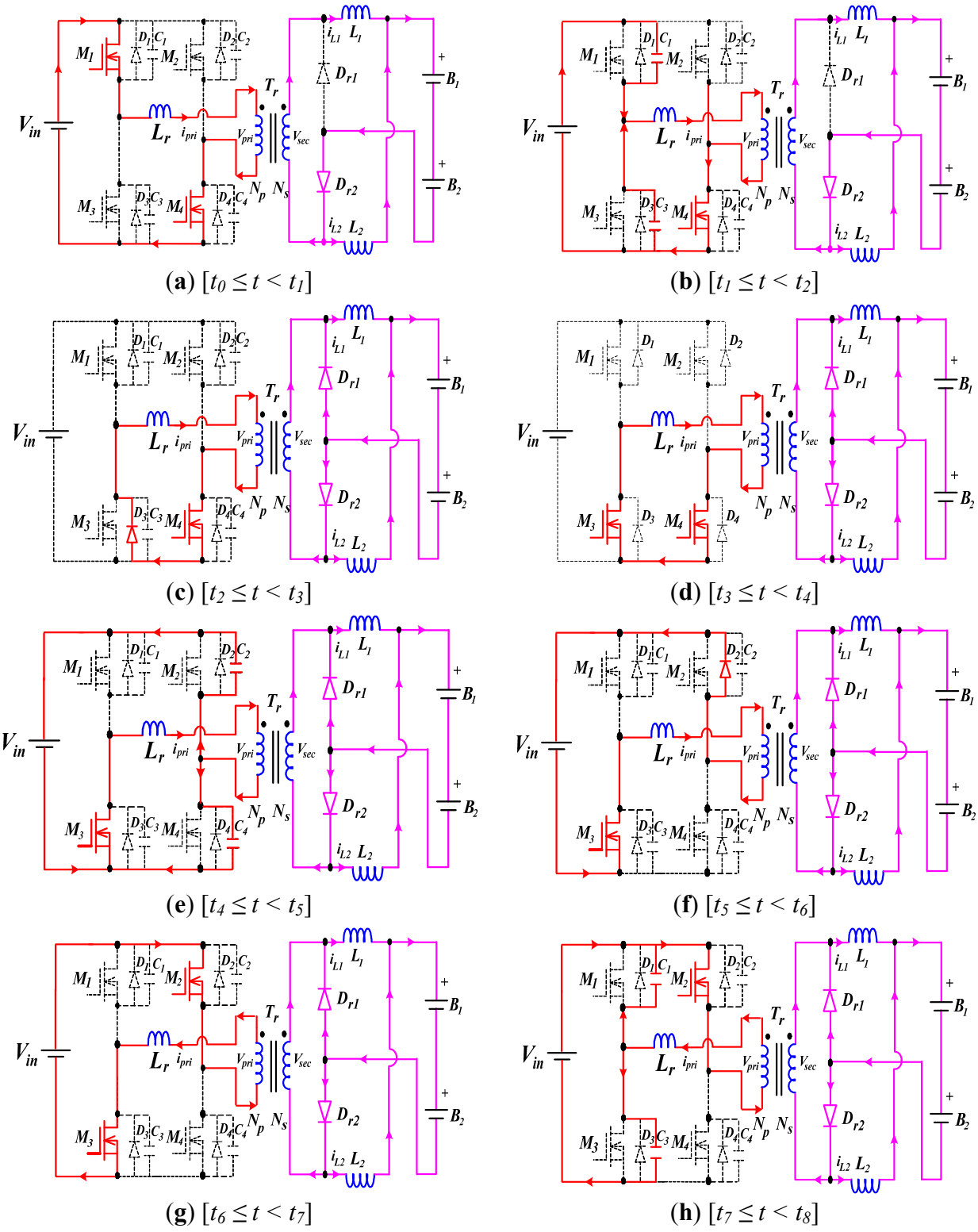

Figure 7. *Cont.*

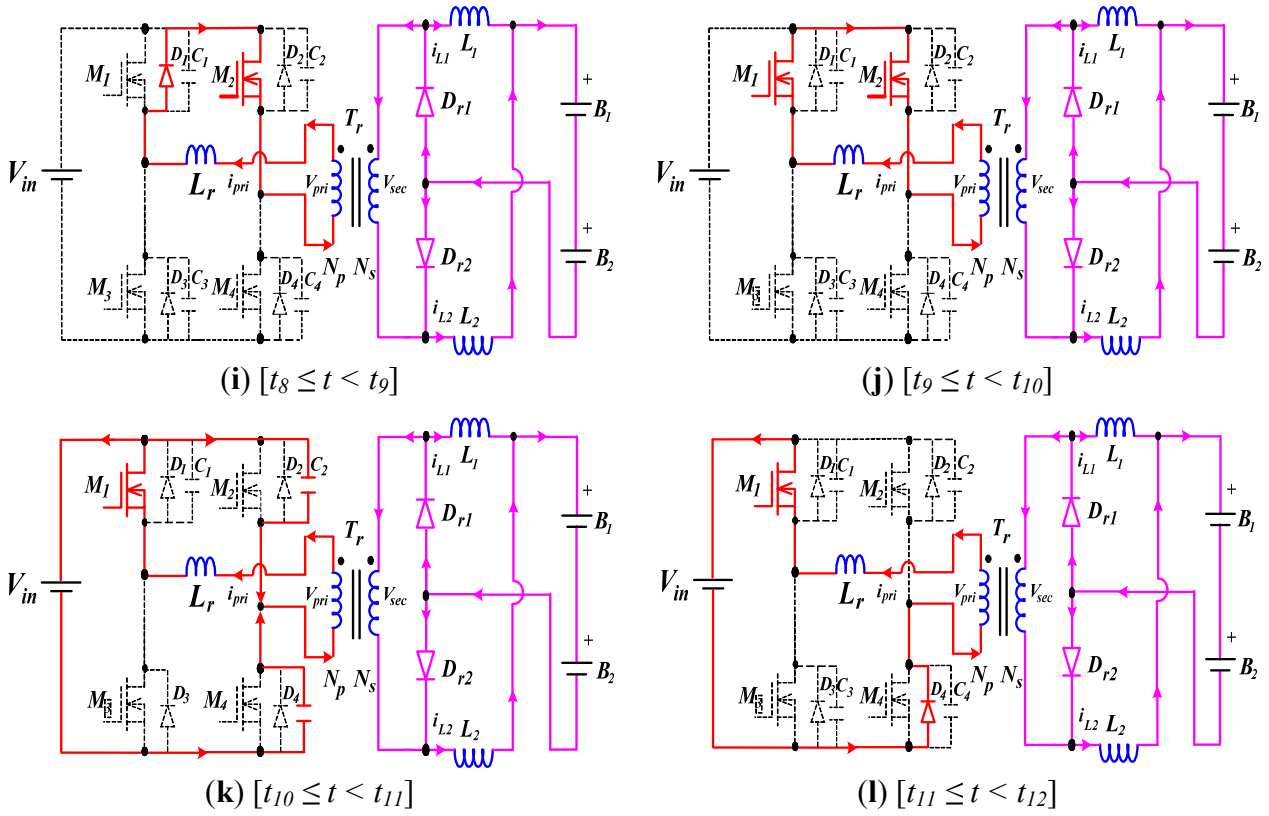

2.2. Operational Principles of Voltage Equalization Mode

In the proposed energy storage system, operation principles of the voltage equalization mode over one switching period can be divided into eight stages. Figure 8 shows conceptual voltage and current waveforms relative to key components of the proposed energy storage system at volatge equalization mode. Figure 9 shows its equivalent circuits.

Stage1 [Figure 9(a), $t_0 \le t < t_1$]:

At time t_0, active switches M_5 is conducted and M_6 is turned off. While the battery B_1 begins discharging, the inductor current i_{LB} flowing through the path M_5-L_B-B_1 is increased linearly.

Stage 2 [Figure 9(b), $t_1 \le t < t_2$]:

At time t_1, the active switch M_5 is turned off and M_6 is maintained off. The parasitic capacitor C_5 of the M_5 is charged to $V_{B1} + V_{B2}$, while the parasitic capacitor C_6 of M_6 is discharged down to zero.

Stage 3 [Figure 9(c), $t_2 \le t < t_3$]:

At time t_2, the The inductor current i_{LB} forces the body diode D_6 of M_6 conducting and creating a ZVS feature for M_6. During this interval, the inductor current flowing through the path B_2-D_6-L_B is linearly decreased. In the stage, the battery B_2 is charged in a short time to create a voltage equalization feature.

Stage 4 [Figure 9(d), $t_3 \le t < t_4$]:

At time t_3, the active switch M_6 is turned on under ZVS transition. During this interval, the inductor current i_{LB} continues decreasing linearly.

Stage 5 [Figure 9(e), $t_4 \le t < t_5$]:

When the inductor current i_{LB} is decreased to zero at time t_4. The battery B_2 begins discharging and inductor current i_{LB} flowing through the path B_2-L_r-M_6 is linearly increased.

Stage 6 [Figure 9(f), $t_5 \le t < t_6$]:

At time t_5, the active switch M_6 is turned off and M_5 is maintained off. The parasitic capacitor C_6 of the M_6 is charged to $V_{B1} + V_{B2}$, while parasitic capacitor C_5 of the M_5 is discharged down to zero.

Stage 7 [Figure 9(g), $t_6 \le t < t_7$]:

The inductor current i_{LB} forces the body diode D_5 of M_5 conducting and creating a ZVS feature for M_5. During this interval, the inductor current i_{LB} flowing through the path B_2-D_6-L_B is linearly decreased.

Stage 8 [Figure 9(h), $t_7 \le t < t_8$]:

At time t_7, the active switch M_5 is turned on under ZVS transition. During this interval, the inductor current i_{LB} continues decreasing linearly. When the inductor current i_{LB} is decreased to zero at time t_8, the voltage equalization operation of battery charger over one switching cycle is completed.

Figure 8. Driving signals of switches (M_5 and M_6) and conceptual current and voltage waveforms of key components for voltage equalization mode.

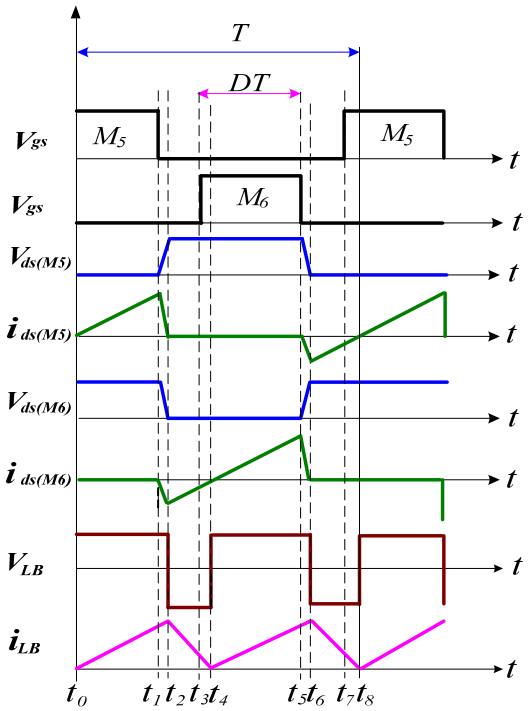

Figure 9. Equivalent circuits of operating stages for voltage equalization mode.

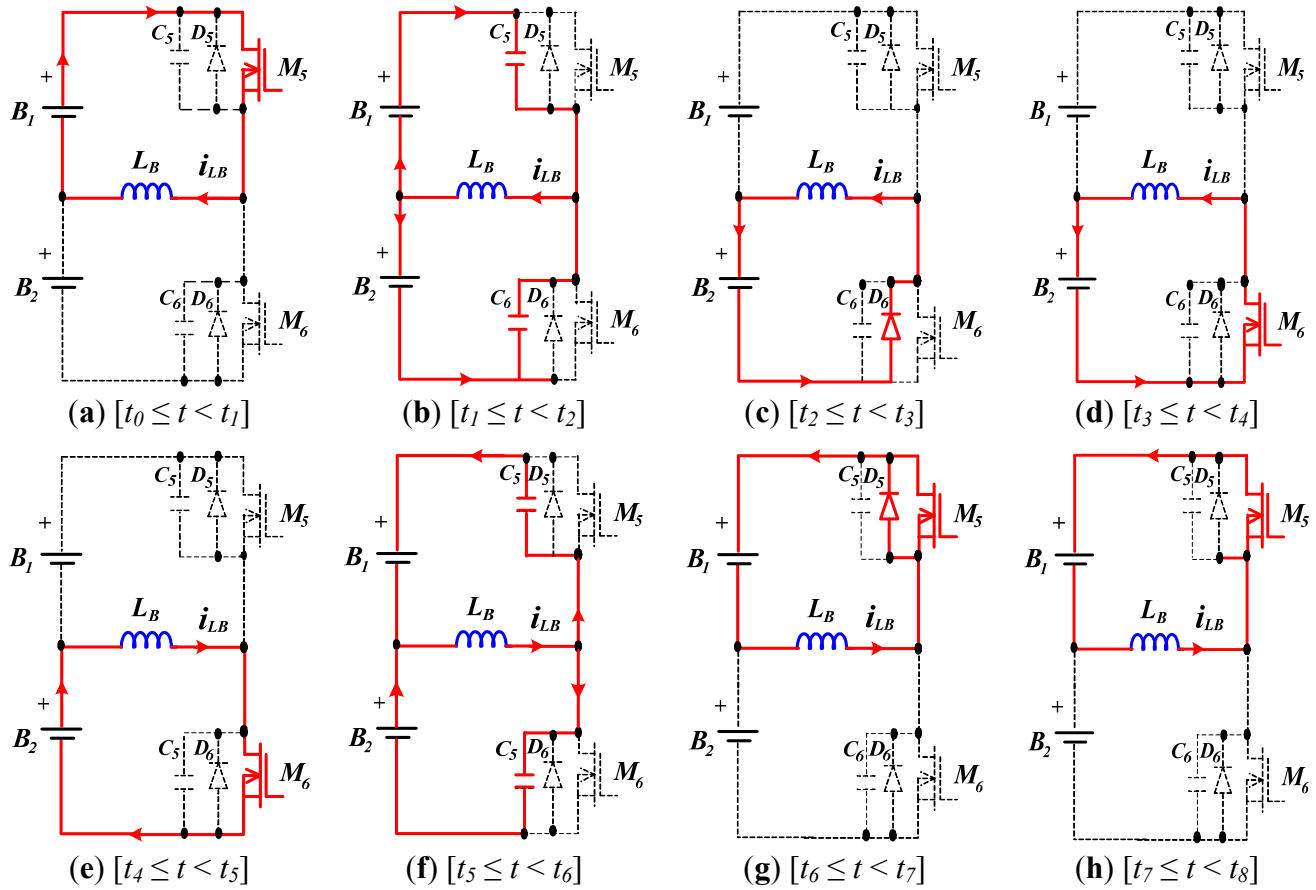

3. Control Scheme

In order to achieve the best energy transfer and control scheme, an MPPT control algorithm and a voltage equalization strategy must be integrated into the proposed energy storage system. In this section, an MPPT algorithm that uses the perturbation and observation method to achieve the best energy utilization of the wind turbine energy and a voltage equalization method will be explained in detail. Furthermore, to achieve an optimal stability and safety for the proposed energy storage system, the functions of under-voltage, over-voltage, over-current, and over-temperature protection circuits are also illustrated.

3.1. Wind Turbine MPPT Algorithm

For experimental convenience, instead of natural wind, a controllable dc motor is used to drive the wind turbine to simulate the actual operating situation under a natural air-stream. Figure 10 shows the emulator simulation system for the wind energy generator. In Figure 10, the dc motor is controlled by different values of dc voltage $V_{dc,motor}$ to provide different limited maximum driving power for driving the wind turbine. When the output power of the wind turbine is small, the dc motor will request small power from the dc voltage $V_{dc,motor}$ to drive the wind turbine. When the speed of the wind turbine increases with generated power, its output voltage along with the rotational speed will be decreased so that the dc motor will generate a larger torque to drive it. Since the limited maximum driving power of the dc motor is predetermined by the dc motor controller, the dc motor can only provide a limited

maximum torque corresponding to the predetermined limited maximum driving power to drive the wind turbine. As a result, the wind turbine can only generate a limited maximum power for the load.

Figure 10. The emulator simulation system for the wind energy generator.

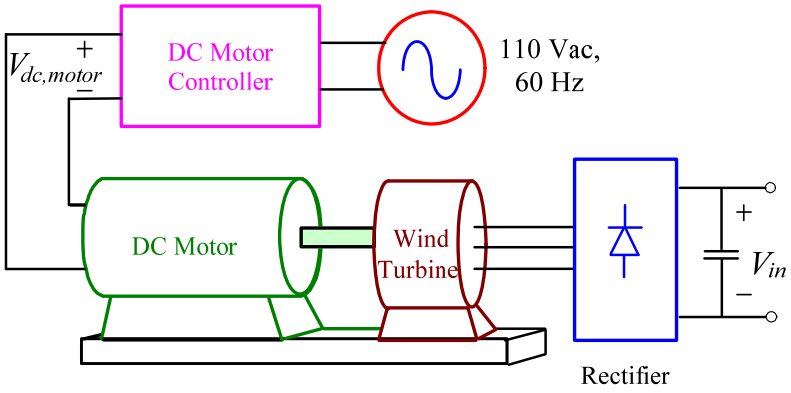

Figure 11 shows the typical output power characteristic curves of the wind turbine under different output voltages. The output power characteristic curves imply that the wind turbine will generate different maximum output powers for different wind speeds. In order to draw the maximum power from the wind energy, the MPPT algorithm adopts the perturbation and observation method. Figure 12 illustrates the flow chart of the MPPT algorithm for the wind energy generator. First of all, the terminal voltage V_{wind} and current I_{wind} of wind turbine are measured. The output power of wind turbine P_{wind} can be obtained from the product of V_{wind} and I_{wind}. The power operating point location can be determined by a perturbation in the wind turbine output power, as shown in Figure 11. The parameters $n-1$ and n of Figure 12 indicate the measured quantities before and after the perturbation, respectively.

Figure 11. Typical output power characteristic curves of the wind turbine under different driving power from the dc motor.

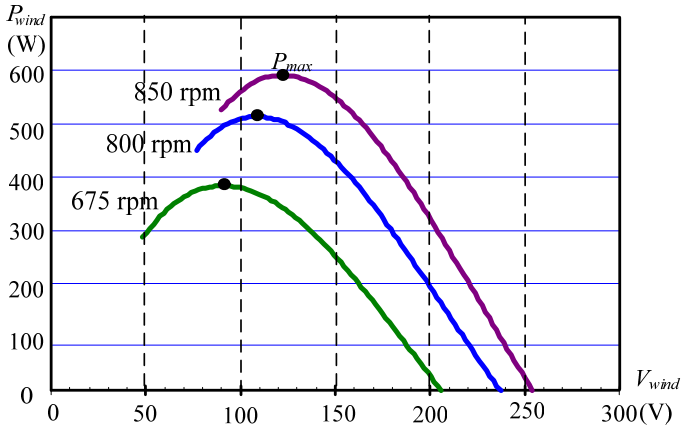

Figure 12. Flow chart of perturbation and observation method for MPPT algorithm.

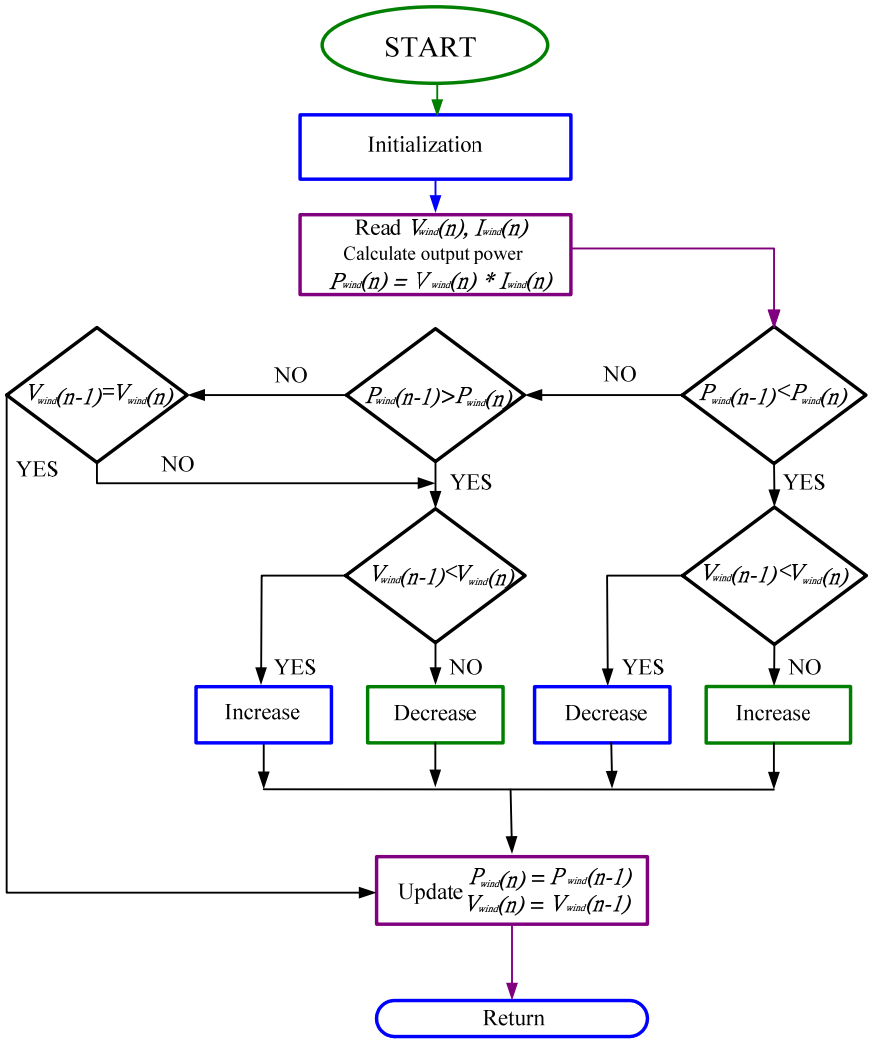

3.2. Control Strategy of Voltage Equalization

Figure 13 shows the proposed non-dissipative charging and voltage equalization strategies. It consists of three operational modes: (1) the charging mode; (2) the inactive rest mode; and (3) the voltage equalization mode. During the active-charge mode, a phase-shift full-bridge converter with continued charging constant currents is applied. Thus, a rest period is used to provide a relaxed time of the series-connected batteries. Finally, in the voltage equalization mode, a series of sharp triangular currents is applied to achieve the voltage equalization and reduce internal temperature of the series-connected batteries.

3.3. Protection Circuits

To achieve an optimal stability and safety for the proposed energy storage system, the functions of under-voltage, over-voltage, over-current, and over-temperature protection circuits are required. All of the protection signals are also realized on the TMS320F240 microcontroller. The conceptual control block diagram of the proposed energy storage system for wind energy conversion is shown in Figure 14. In Figure 14, the control circuits of the proposed energy storage system are implemented on

microcontroller along with auxiliary analog circuits. The front-end is used phase-shift full-bridge converter by microcontroller to draw maximum power from the wind turbine, while the rear-end is used non-dissipative voltage equalization circuit to control the voltage equalization of the batteries. The output voltages and currents of the wind turbine are sensed, and sent to the microcontroller where the MPPT algorithm will determine the reference currents $I_{wind,ref}$ and $V_{wind,ref}$ corresponding to the maximum power of wind turbine at that moment for wind-turbine output current I_{in} and V_{in} to keep up with. By comparing these signals, the PWM comparator will generate desired gate driving signals of active switches (M_1, M_2, M_3, and M_4) realize the MPPT functions.

Figure 13. The proposed non-dissipative charging and voltage equalization strategies.

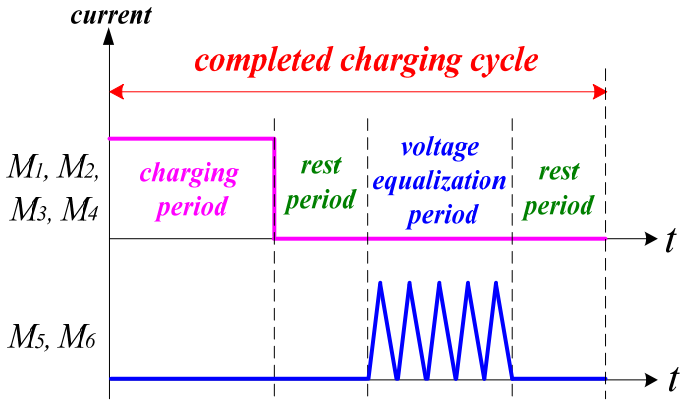

Figure 14. Conceptual control block diagram of the proposed energy storage system for wind energy conversion.

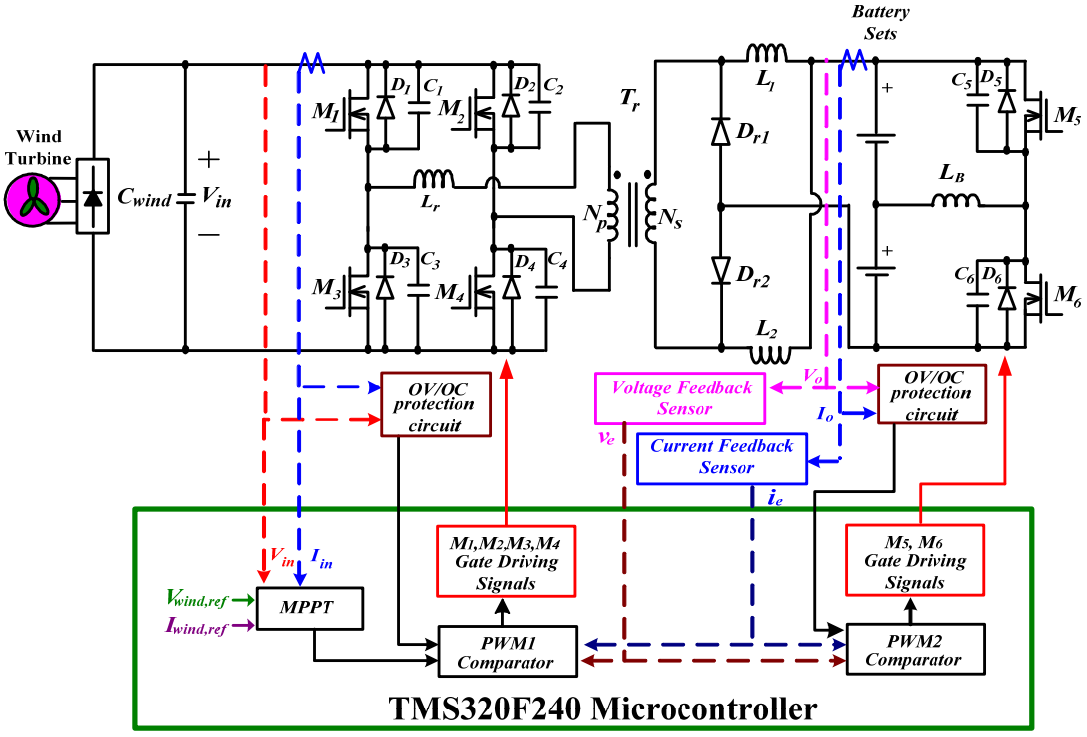

3.4. Condition of ZVS

In order to reduce the switching losses of the active switches (M_1, M_2, M_3 and M_4), the phase-shift full-bridge converter is necessary to store enough energy in the resonant inductor L_r to achieve ZVS at switches turn-on transition. The ZVS condition for four active switches can be obtained from the following inequality:

$$L_r \geq \frac{(C_1 // C_3)\ (V_{in})^2}{(i_{pri})^2} = \frac{(C_2 // C_4)\ (V_{in})^2}{(i_{pri})^2} \tag{1}$$

When the value of the parasitic capacitors is equal ($C_1 = C_2 = C_3 = C_4 = C$), the inequality can be expressed as follows:

$$L_r \geq \frac{2C\ (V_{in})^2}{(i_{pri})^2} \tag{2}$$

If the value of active switches (M_1~M_4) is selected so that a proper resonant inductor L_r can be obtained. In inequality (2), for determining resonant inductor L_r, we can plot the curves showing the relationship between resonant inductor L_r and input currents i_{pri} under different input voltages, as illustrated in Figure 15. The resonant inductor should be selected from the gray area for achieving ZVS.

Figure 15. Plots of the ZVS region relating to resonant inductor L_r and input current ipriunder different input voltage.

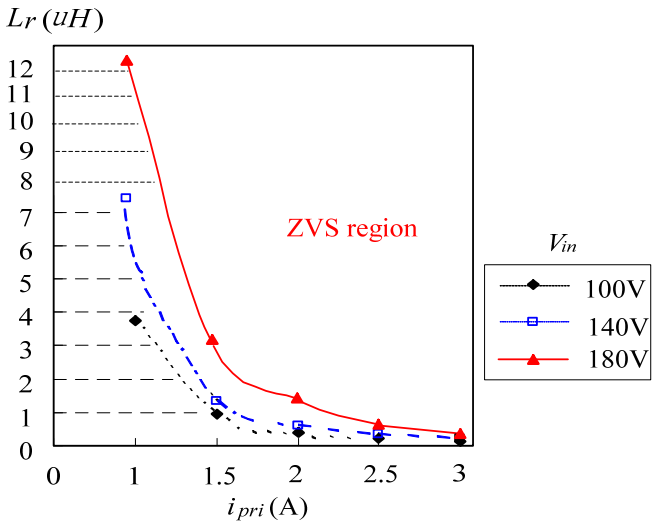

Similarly, the non-dissipative voltage equalization circuit is also necessary to store enough energy in the inductor L_B to achieve ZVS at switches turn-on transition. Usually, the function of inductor L_B is designed to achieve the voltage equalization of the series batteries. The relationship of the inductor L_B and battery voltage can be obtained as following equation:

$$L_B = \frac{(1-D)}{2f_s}\left(\frac{V_B}{i_{LB}}\right) \tag{3}$$

where D and f_s are the duty ratio and switching frequency of the active switches (M_5 and M_6). From (3), the proper value of the inductor L_B can be determined to achieve the voltage equalization of the series

batteries. Therefore, the energy of the inductor L_B is enough to achieve ZVS at the switches turn-on transition of the active switches (M_5 and M_6).

Figure 16. Experimental circuit of the proposed energy storage system.

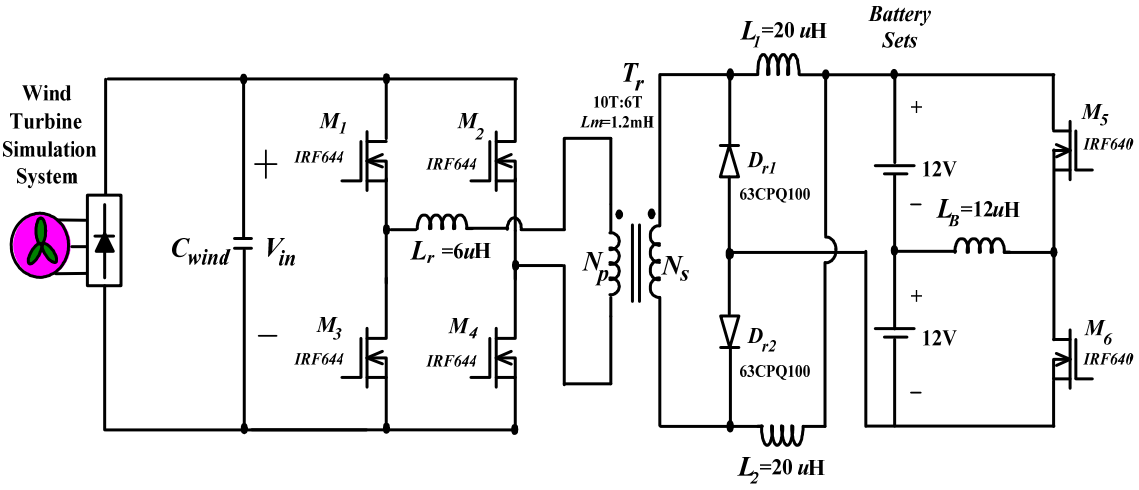

4. Experimental Results

The key component values of the experimental circuit used to verify the performance of the proposed energy storage system for wind energy conversion are shown in Figure 16 and its specifications are listed as follows: the Bergey BWC XL.1 emulator simulation system for the wind energy generator is used. It is a three-phase permanent magnetic generator with rated power of 600 W at rated wind speed of 11 m/s,

(1) Input voltage: V_{in} = 80~180 V_{dc};
(2) Output voltage of series batteries: V_{out} = 24 V_{dc};
(3) Maximum charging current of series batteries: $i_B = i_{L1} + i_{L2}$ = 20 A;
(4) Discharging current of series batteries: i_{LB} = 10 A;
(5) Inductors L_1 and L_2 = 20 μH, L_B = 12 μH;
(6) Resonant Inductors L_r = 6 μH;
(7) Switching frequency: fs = 50 kHz (M_1~M_6).

Figure 17 shows measured output currents, voltages and their corresponding powers from start-up to the steady state for wind turbine energy with MPPT algorithm. From Figure 17, it can be observed that the perturbation and observation method for the wind turbine energy can be always obtained from maximum power point. Figure 18 shows measured primary current and voltage waveforms of transformer. Figure 19 shows measured current waveforms of inductors L_1 and L_2, from which it can be seen that the inductor currents i_{L1} and i_{L2} have an interleaved feature. Thus, the ripples of output current can be reduced. Figure 20 shows power switches M_1 and M_4 to illustrate a ZVS feature, respectively. Figure 21 shows measured voltage and current waveforms of inductors L_B for voltage equalization of series-connected batteries. Figure 22 shows measured voltage and current waveforms of power switch (M_5 or M_6), from which it can be seen that the switch (M_5 or M_6) has a ZVS feature at turn-on transition. Figure 23 shows the comparison between voltage equalization measurements of

series-connected batteries B_1 and B_2 under the condition of voltage imbalance ($V_{B1} > V_{B2}$ and $V_{B1} < V_{B2}$), from which it can be seen that the series-connected batteries can be improved in a short time by the proposed voltage equalization strategy.

Figure 17. Measured output voltage, current and power waveforms of wind turbine with MPPT algorithm. V_{wind}: 100 V/div; P_{wind}: 200 W/div; I_{wind}: 1 A/div; time: 5 s/div.

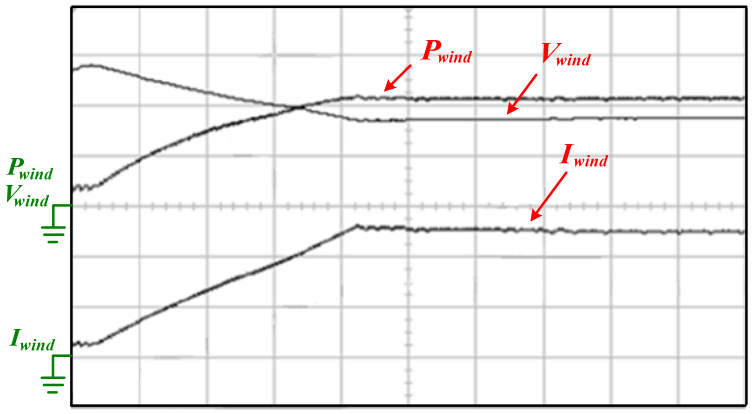

Figure 18. Measured primary voltage and current waveforms of transformer. V_{pri}: 100 V/div; i_{pri}: 2 A/div; time: 5 μs/div.

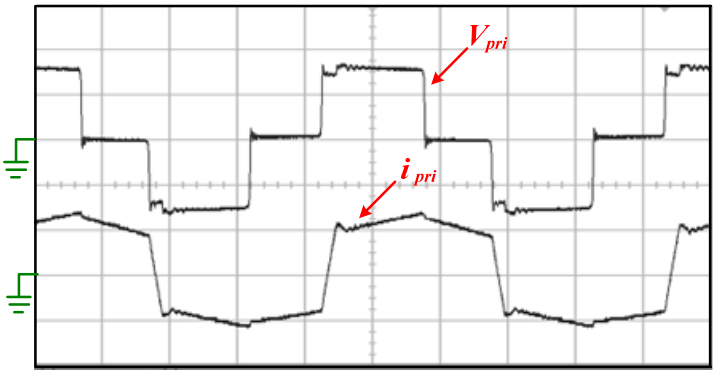

Figure 19. Measured current waveforms of inductors (L_1 and L_2) for current-doubler rectifier. i_{L1}, i_{L2}: 5 A/div; time: 2 μs/div.

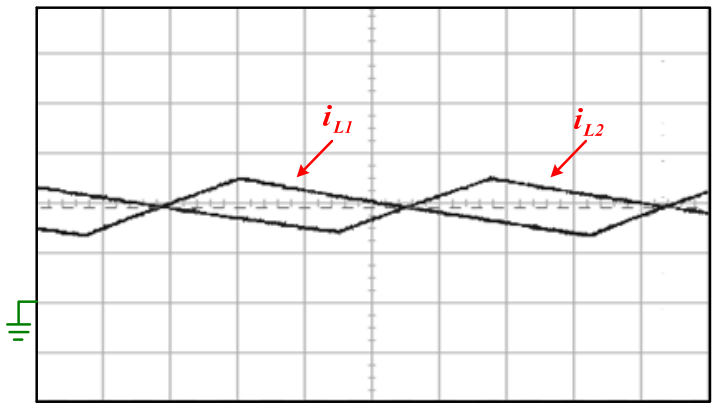

Figure 20. Measured current waveforms of power switches (M_1 and M_2) and primary voltage waveforms of transformer for phase-shift full-bridge converter. i_{M1}, i_{M4}: 2 A/div; V_{pri}: 100 V; time: 10 μs/div.

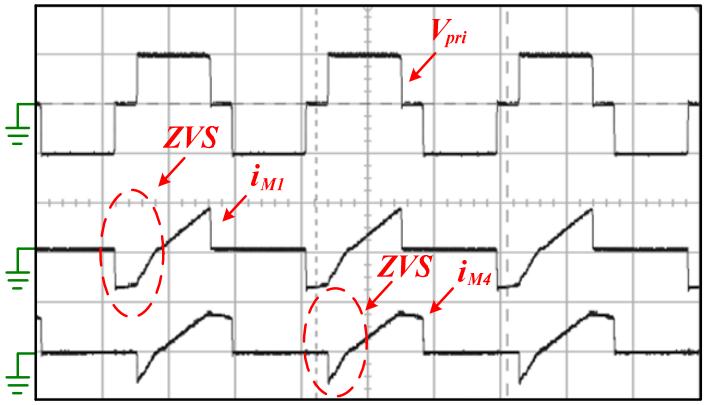

Figure 21. Measured voltage and current waveforms of inductor L_B. V_{LB}: 50 V/div; i_{LB}: 5 A/div time: 10 μs/div. For non-dispassive voltage equalization circuit.

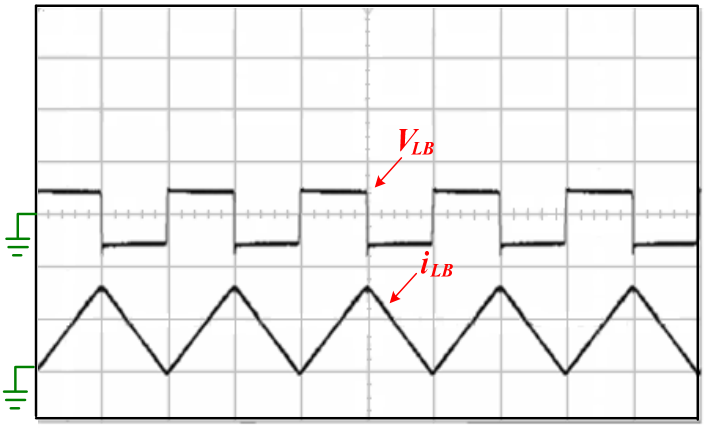

Figure 22. Measured voltage and current waveforms of power switch (M_5 or M_6) for non-dispassive voltage equalization circuit. V_{ds}: 20 V/div; i_{ds}: 5 A/div; time: 2 μs/div.

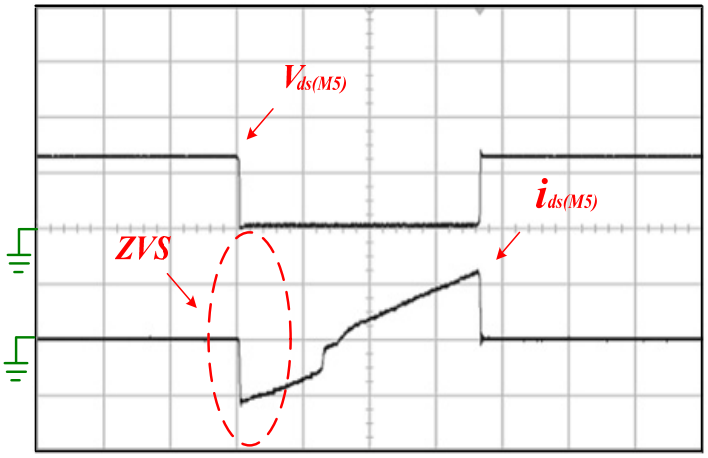

Figure 23. Measured voltage equalization curves of series-connected batteries B_1 and B_2 under voltage imbalance condition: **(a)** $V_{B1} > V_{B2}$; **(b)** $V_{B1} < V_{B2}$.

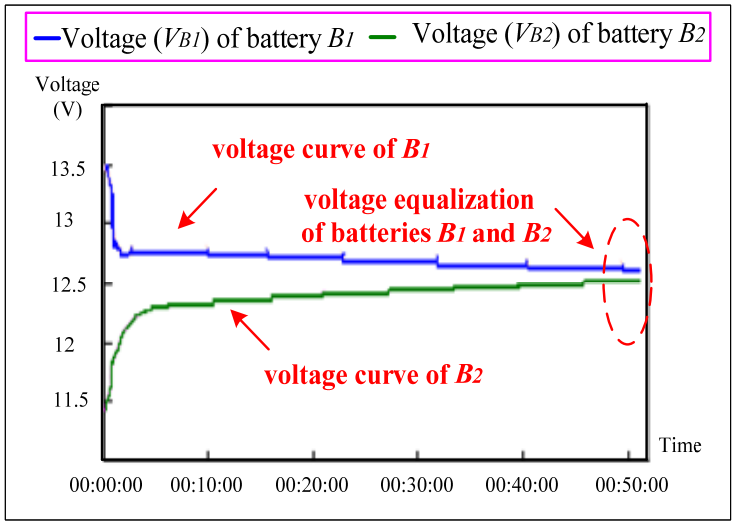

(a)

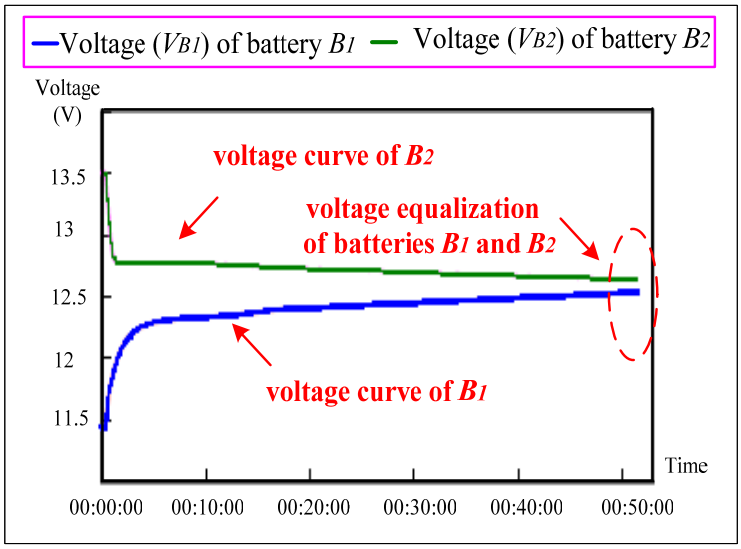

(b)

5. Conclusions

In this paper, an energy storage system with voltage equalization strategy for wind energy conversion is proposed. All power switches of the proposed energy storage system have a ZVS feature at turn-on transition. Hence, the switching losses of the power switches can be reduced. In order to draw maximum power from the wind turbine energy, a simple perturbation and observation method is incorporated to realize maximum power conversion. To adopt a cost effective of the proposed energy storage system, the MPPT algorithms and protected circuits consist of a digital signal processor (DSP) and analog circuits to implement maximum power conversion and protect the system. Thus, the control circuit of the proposed energy storage system is compact and programmable. Experimental results have verified that the proposed energy storage system is suitable for wind energy conversion.

References

1. Bull, S.R. Renewable energy today and tomorrow. *Proc. IEEE* **2001**, *89*, 1216–1226.
2. World Wind Energy Association. World Wind Energy Report 2008. Available online: http://www.wwindea.org/home/images/stories/worldwindenergyreport2008_s.pdf (accessed on 2 July 2012)
3. Robinson, J.; Jovcic, D.; Joos, G. Analysis and design of an offshore wind farm using a MV dc grid. *IEEE Trans. Power Deliv.* **2010**, *25*, 2164–2173.
4. O'Donnell, R.; Schofield, N.; Smith, A.C.; Cullen, J. Design Concepts for High-Voltage Variable-Capacitance DC Generators. *IEEE Trans. Ind. Appl.* **2009**, *45*, 1778–1784.
5. Rahimi, M.; Parniani, M. Efficient control scheme of wind turbines with doubly fed induction generators for low-voltage ride-through capability enhancement. *Renew. Power Gener.* **2010**, *4*, 242–252.
6. Teleke, S.; Baran, M.E.; Huang, A.Q.; Bhattacharya, S.; Anderson, L. Control Strategies for Battery Energy Storage for Wind Farm Dispatching. *IEEE Trans. Energy Convers.* **2009**, *24*, 725–731.
7. Kuo, Y.C.; Liang, T.J.; Chen, J.F. Novel maximum-power-point-tracking controller for photovoltaic energy conversion system. *IEEE Trans. Ind. Electron.* **2001**, *48*, 594–601.
8. Koyanagi, A.; Nakamura, H.; Kobayashi, M.; Suzuki, Y.; Shimada, R. Study on maximum power point tracking of wind turbine generator using a flywheel. *Proc. Power Convers.* **2002**, *1*, 322–327.
9. Amei, K.; Takayasu, Y.; Ohji, T.; Sakui, M. A maximum power control of wind generator system using a permanent magnet synchronous generator and a boost chopper circuit. *Proc. Power Convers.* **2002**, *3*, 1447–1452.
10. Patel, H.; Agarwal, V. MPPT Scheme for a PV-Fed Single-Phase Single-Stage Grid-Connected Inverter Operating in CCM with Only One Current Sensor. *IEEE Trans. Energy Convers.* **2009**, *24*, 256–263.
11. Moore, S.W.; Schneider, P.J. A Review of Cell Equalization Methods for Lithium Ion and Lithium Polymer Battery System. In *Proceedings of Society of Automotive Engineers 2001 World Congress*, Detroit, MI, USA, March 2001.
12. Cao, J.; Schofield, N.; Emadi, A. Battery Balancing Methods: A Comprehensive Review. In *Proceedings of IEEE Vehicle Power and Propulsion Conference*, Harbin, China, September 2008.
13. Cho, J.G.; Baek, J.W.; Jeong, C.Y.; Rim, G.H. Novel Zero-Voltage and Zero- Current-Switching Full Bridge PWM Converter Using Transformer Auxiliary Winding. *IEEE Trans. Power Electron.* **2000**, *15*, 250–257.
14. Lee, Y.S.; Chen, G.T. Bi-directional DC-to-DC Converter Application in Battery Equalization for Electric Vehicles. In *Proceedings of IEEE Power Electronics Specialists Conference*, Aachen, Germany, June 2004; pp. 2766–2772.

15. Lee, Y.S.; Chen, M.W; Hsu, K.L.; Du, J.Y.; Chuang, C.F. Cell Equalization Scheme with Energy Transferring Capacitance for series connected battery strings. In *Proceedings of IEEE Region 10 Technical Conference on Computers, Communications, Control and Power Engineering (IEEE TENCON'02)*, Beijing, China, October 2002; pp. 2042–2045.